

Path loss exponent estimation for wireless sensor network localization

Guoqiang Mao^{a,*}, Brian D.O. Anderson^b, Barış Fidan^b

^a *University of Sydney and National ICT Australia, Sydney, Australia*

^b *Australian National University and National ICT Australia, Canberra, Australia*

Received 1 April 2006; received in revised form 3 September 2006; accepted 5 November 2006

Available online 29 November 2006

Responsible Editor: S. Palazzo

Abstract

The wireless received signal strength (RSS) based localization techniques have attracted significant research interest for their simplicity. The RSS based localization techniques can be divided into two categories: the distance estimation based and the RSS profiling based techniques. The path loss exponent (PLE) is a key parameter in the distance estimation based localization algorithms, where distance is estimated from the RSS. The PLE measures the rate at which the RSS decreases with distance, and its value depends on the specific propagation environment. Existing techniques on PLE estimation rely on both RSS measurements and distance measurements in the same environment to calibrate the PLE. However, distance measurements can be difficult and expensive to obtain in some environments. In this paper we propose several techniques for online calibration of the PLE in wireless sensor networks without relying on distance measurements. We demonstrate that it is possible to estimate the PLE using only power measurements and the geometric constraints associated with planarity in a wireless sensor network. This may have a significant impact on distance-based wireless sensor network localization.

© 2006 Elsevier B.V. All rights reserved.

Keywords: Sensor network; Path loss exponent; Cayley–Menger determinant; Data fusion

1. Introduction

Most wireless sensor network (WSN) applications require knowing or measuring locations of thousands of sensors accurately. In environmental sensing applications such as bush fire surveillance, water quality monitoring and precision agriculture,

for example, sensing data without knowing the sensor location is meaningless [1]. In addition, location estimation may enable applications such as inventory management, intrusion detection, road traffic monitoring, health monitoring, etc.

Sensor network localization estimates the locations of sensors with unknown location information with regards to a few sensors with known location information by using inter-sensor measurements such as distance and bearing measurements. Inter-sensor measurement techniques in WSN localization

* Corresponding author. Tel.: +61 2 93512962; fax: +61 2 93513847.

E-mail address: g.mao@ieee.org (G. Mao).

can be broadly classified into three categories: received signal strength (RSS) measurements, angle of arrival (AOA) measurements, and propagation time based measurements. Among them, RSS based localization techniques have received considerable research interest [1–8]. Although RSS based localization techniques can only provide a coarse-grained location estimate, they are attractive because of their simplicity. Received signal strength indicator (RSSI) has become a standard feature in most wireless devices, therefore RSS based localization techniques require no additional hardware, and are unlikely to significantly impact local power consumption, sensor size and thus cost. RSS based localization techniques can be further divided into distance-estimation based [1,3–6] and RSS-profiling based techniques [2,7,9,10].

Existing distance-estimation based techniques rely on a log-normal radio propagation model [11] to estimate inter-sensor distances from RSS measurements. The path loss exponent (PLE) is a key parameter in the log-normal model. An accurate knowledge of the PLE is required in order to obtain an accurate estimate of the inter-sensor distance from the corresponding RSS measurement. Existing techniques either consider the PLE is known a priori by assuming the WSN environment is free space, or obtain the PLE through extensive channel measurement and modeling by measuring both RSS and distances in the same environment of WSN prior to system deployment. However, the PLE is environment dependent. Even in the same environment, the channel characteristics may change considerably over a long period of time due to seasonal changes and weather changes [11]. Therefore, it is an oversimplification to assume a free space environment. On the other hand a priori channel measurement and modeling may not be possible for monitoring and surveillance applications in hostile or inaccessible environments. In this paper, we propose several techniques for online calibration of the path loss exponent, which do not rely on distance measurements.

The RSS has been popularly modeled by a log-normal model [1,11–13]:

$$P_{ij} [\text{dBm}] \sim N(\overline{P}_{ij} [\text{dBm}], \sigma_{\text{dB}}^2), \quad (1)$$

$$\overline{P}_{ij} [\text{dBm}] = P_0 [\text{dBm}] - 10 \times \alpha \times \log_{10}(d_{ij}/d_0), \quad (2)$$

where $P_{ij} [\text{dBm}]$ is the received power at a receiving node j from a transmitting node i in dB milliwatts, $\overline{P}_{ij} [\text{dBm}]$ is the mean power in dB milliwatts, σ_{dB}^2

is the variance of the shadowing, $P_0 [\text{dBm}]$ is the received power in dB milliwatts at a reference distance d_0 , and d_{ij} is the distance between nodes i and j . In this paper, we use the notation $[\text{dBm}]$ to denote that power is measured in dB milliwatts. Otherwise, it is measured in milliwatts. The reference power $P_0 [\text{dBm}]$ is calculated using the free space Friis equation or obtained through field measurements at the reference distance d_0 [11]. It is important to note that the reference distance d_0 should be in the far field of the transmitter antenna so that the near-field effect does not alter the reference power. In large coverage cellular systems, a 1 km reference distance is commonly used, whereas in microcellular systems, a much smaller distance such as 100 m or 1 m is used [11]. In this paper, it is assumed that d_0 and $P_0 [\text{dBm}]$ can be obtained from a priori calibration of the wireless device and they are known constants. In many situations, $P_{ij} [\text{dBm}] \neq P_{ji} [\text{dBm}]$ due to the asymmetric wireless signal propagation path from node i to node j and from node j to node i . However, in this paper, it is assumed that $P_{ij} [\text{dBm}] = P_{ji} [\text{dBm}]$ for simplicity. In the case of an asymmetric path, the average value of $P_{ij} [\text{dBm}]$ and $P_{ji} [\text{dBm}]$ is used [1]. It is also assumed that all distances are normalized with respect to d_0 .

The parameter α is called the path loss exponent, which measures the rate at which the received signal strength decreases with distance. The value of α depends on the specific propagation environment. In this paper, it is assumed that α is an unknown constant, which needs to be determined. For a large wireless sensor network spanning a wide area with different environmental conditions, the area can be divided into smaller regions and α can be considered as a constant in each region. Path loss exponent estimation plays an important role in distance-based wireless sensor network localization, where distance is estimated from the received signal strength measurements [14]. Path loss exponent estimation is also useful for other purposes like sensor network dimensioning. As the value of the path loss exponent depends on the environment in which a sensor network is deployed, existing techniques on path loss exponent estimation rely on both RSS measurements and distance measurements (obtained using a method other than from the RSS, e.g., by using a ruler) in the same environment to calibrate the path loss exponent [1,13]. RSS measurements are readily available. However, distance measurements can be difficult and expensive to obtain in some environments. Moreover, the reliance on distance

measurements impedes deployment in unknown environments.

In this paper, we propose several techniques for online calibration of the path loss exponent, which do not rely on distance measurements. The proposed technique also does not assume knowledge of the quantity σ_{dB}^2 in Eq. (1). We demonstrate that it is possible to estimate the PLE using only power measurements and the geometric constraints associated with planarity in a sensor network. This may have a significant impact on distance-based wireless sensor network localization. For ease of explanation, this paper focuses on path loss exponent estimation in 2D. However the proposed technique may also be extended to 3D.

The rest of the paper is organized as follows. In Section 2, we present a technique which estimates the path loss exponent based on known probability distribution of inter-sensor distances. In Section 3, we present the principle of the path loss exponent estimation using the Cayley–Menger determinant [15,16]. Sections 4 and 5 present the proposed algorithm and an improvement of it using data fusion. Both algorithms do not rely on knowledge of distance-related information. The validity of these algorithms is established using simulation and real measurement data. Finally, conclusions and suggestions for further work are summarized in Section 6.

2. Path loss exponent estimation based on known probability distribution of inter-sensor distances

In this section, we consider the estimation of the path loss exponent assuming that the probability distribution of distance between neighboring sensors is known. In some applications, it is possible to know a priori the probability distribution of distance between neighboring sensors. For example, Stoleru and Stankovic [17] consider that in some applications like precision agriculture, sensors will be deployed approximately on the grid points with some error. In that case, the approximate probability distribution of distance between neighboring sensors can be obtained by assuming a certain distribution of the error, e.g., Gaussian distribution. Some other researchers also consider the deployment of sensors near grid points [18,19]. In addition, it is possible to obtain an accurate knowledge of the probability distribution of inter-sensor distances from the distribution of wireless sensors [20–22]. In particular, it was shown in [20] that under certain conditions, the inter-sensor distance distributions

are very similar when sensors are distributed in the region following a uniform distribution or a Gaussian distribution.

If the distribution has a simple form allowing straightforward computation, the method of moments estimator [23, Section 12.6] can be used to obtain the path loss exponent estimate. For example, if the distance between neighboring nodes is uniformly distributed in the range $[a, b]$, using Eqs. (1) and (2) the expected value of the measured power can be obtained:

$$E(P_{ij} [\text{dBm}]) = \int_a^b P_0 [\text{dBm}] - 10 \times \alpha \times \log_{10} x dx, \quad (3)$$

$$= P_0 [\text{dBm}](b - a) - \frac{10 \times \alpha}{\ln 10} [-x + x \ln x]_a^b. \quad (4)$$

An estimate of α can be obtained by equating the expected value of $P_{ij} [\text{dBm}]$ with the sample mean of the measured received power. In this paper, we assume that all sensors radiate at the same power level for simplicity, i.e., $P_0 [\text{dBm}]$ is the same for all sensors. However, the derivation in this paper does not rely on this assumption but rather the weaker assumption that the receiver knows the exact value of the radiated power of the transmitter.

A more generic technique, based on the same idea as the quantile–quantile (q–q) plot [24], can be used if the distance distribution has a complex form which is not suitable for computation. The q–q plot is a graphical technique for determining whether two data sets come from populations with a common distribution. Using an approach similar to the q–q plot, a set of points $\lambda_1, \lambda_2, \dots, \lambda_N$ uniformly distributed in the interval $(0, 1)$ is selected. The quantile points of the distance distribution d_1, d_2, \dots, d_N and the measured received power $P_1 [\text{dBm}], P_2 [\text{dBm}], \dots, P_N [\text{dBm}]$ corresponding to $\lambda_1, \lambda_2, \dots, \lambda_N$ can then be determined, where

$$d_i = \arg\{Pr(d \geq d_i) = \lambda_i\}, \quad (5)$$

and

$$P_i [\text{dBm}] = \arg\{Pr(P [\text{dBm}] \leq P_i [\text{dBm}]) = \lambda_i\}. \quad (6)$$

An estimate of α can be obtained by minimizing the function $f(\hat{\alpha})$:

$$f(\hat{\alpha}) = \sum_{i=1}^N (P_i [\text{dBm}] - P_0 [\text{dBm}] + 10 \times \hat{\alpha} \log_{10} d_i)^2. \quad (7)$$

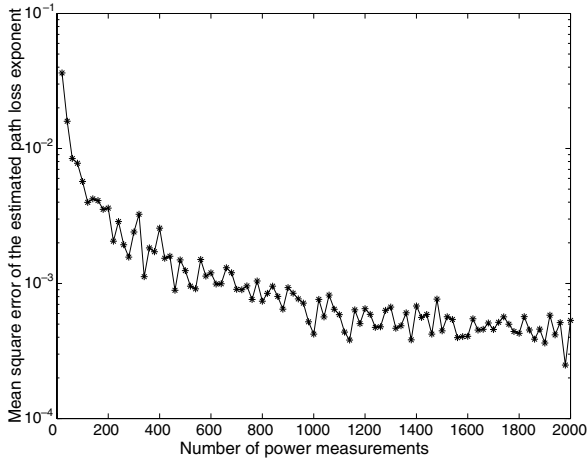


Fig. 1. Variation of the mean square error of $\hat{\alpha}$ with the number of power measurements.

Differentiating $f(\hat{\alpha})$ and setting it to be zero, the value of $\hat{\alpha}$ can be obtained:

$$\hat{\alpha} = \frac{-\sum_{i=1}^N (P_i [\text{dBm}] - P_0 [\text{dBm}]) \log_{10} d_i}{\sum_{i=1}^N 10(\log_{10} d_i)^2}. \quad (8)$$

Fig. 1 shows the variation of the mean square error of the estimated path loss exponent $\hat{\alpha}$ with the number of power measurements. The mean square error is obtained by running the simulation 100 times with the same number of power measurements but using different random seed. The parameters used in the simulation are: the true value of α is 2.3; $\sigma_{\text{dB}} = 3.92$; $P_0 [\text{dBm}] = -37.4603 \text{ dBm}$; $d_0 = 1 \text{ m}$. The distances d_{ij} are uniformly distributed in the interval $[1, 18]$. These parameters are drawn from real measurement data reported in [1]. As shown in the figure, this method is very accurate and $\hat{\alpha}$ converges to the true value very quickly. When the number of power measurements is greater than 200, the mean square error drops below 0.003.

The result shown in Fig. 1 is obtained based on the assumption that the probability distribution of distance between neighboring sensors is known accurately. This may not be the case in real applications. Further work needs to be done on investigating the sensitivity of the aforementioned technique with respect to inaccurate knowledge of the probability distribution of inter-sensor distances.

3. General principle of path loss exponent estimation using the Cayley–Menger determinant

In the last section, we presented a path loss estimation technique based on the knowledge of the

probability distribution of inter-sensor distance. It can calibrate the path loss exponent accurately. However, the proposed technique relies on the knowledge of distance distribution, which can be unrealistic to obtain in some applications. This disadvantage of the proposed technique motivates us to find a more generic technique for path loss exponent estimation without relying on knowledge of the distance distribution, let alone the distance itself. The techniques we present in the following sections also do not assume knowledge of the quantity σ_{dB}^2 in Eq. (1).

Consider a sensor with three neighbors and the neighbors of that sensor are also neighbors of each other. Two sensors i and j are neighbors if P_{ij} is non-zero. The sensor and its neighbors can be represented by a full-connected planar quadrilateral shown in Fig. 2. The tuple (P_{ij}, d_{ij}) represents the measured power and the true distance between node i and node j , respectively. P_{ij} and d_{ij} are related through Eqs. (1) and (2). The path loss exponent estimation problem can be formulated as the simultaneous estimation of the true distances $d_{12}, d_{13}, d_{14}, d_{23}, d_{24}, d_{34}$ and α given the power measurements $P_{12}, P_{13}, P_{14}, P_{23}, P_{24}, P_{34}$. Using the maximum likelihood estimator (MLE), the likelihood function can be obtained as

$$\begin{aligned} L(d_{12}, d_{13}, d_{14}, d_{23}, d_{24}, d_{34}, \alpha) &= \frac{1}{(\sqrt{2\pi}\sigma_{\text{dB}})^6} \prod_{1 \leq i < j \leq 4} \\ &\times \exp\left(-\frac{(P_{ij} [\text{dBm}] - P_0 [\text{dBm}] + 10\alpha \log_{10} d_{ij})^2}{\sigma_{\text{dB}}^2}\right). \end{aligned} \quad (9)$$

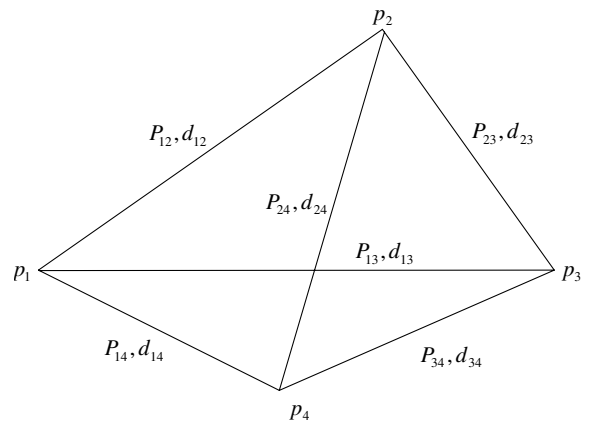


Fig. 2. A fully-connected planar quadrilateral in sensor networks.

Maximizing L is equivalent to minimizing $g(d_{12}, d_{13}, d_{14}, d_{23}, d_{24}, d_{34}, \alpha)$, where

$$g(d_{12}, d_{13}, d_{14}, d_{23}, d_{24}, d_{34}, \alpha) = \sum_{1 \leq i < j \leq 4} (P_{ij} [\text{dBm}] - P_0 [\text{dBm}] + 10\alpha \log_{10} d_{ij})^2. \quad (10)$$

As the number of power measurements is smaller than the number of parameters to be estimated, minimizing g gives us a set of simple equations. In these equations P_{ij} and P_0 are in decimal units, not in dB units, so that $P_{ij} = 10^{P_{ij} [\text{dBm}]/10}$.

$$P_{ij} = P_0 \times d_{ij}^{-\alpha}, \quad 1 \leq i < j \leq 4. \quad (11)$$

Another constraint that is required to solve the above equations can be found from the geometric constraint on a fully-connected planar quadrilateral using the Cayley–Menger determinant [15,16]. The Cayley–Menger determinant of a quadrilateral is given by:

$$D(p_1, p_2, p_3, p_4) = \begin{vmatrix} 0 & d_{12}^2 & d_{13}^2 & d_{14}^2 & 1 \\ d_{12}^2 & 0 & d_{23}^2 & d_{24}^2 & 1 \\ d_{13}^2 & d_{23}^2 & 0 & d_{34}^2 & 1 \\ d_{14}^2 & d_{24}^2 & d_{34}^2 & 0 & 1 \\ 1 & 1 & 1 & 1 & 0 \end{vmatrix} \quad (12)$$

A classical result on the Cayley–Menger determinant is given by the following theorem.

Theorem 1 (Theorem 112.1 in [16]). *Consider an n -tuple of points p_1, \dots, p_n in m -dimensional space with $n \geq m + 1$. The rank of the Cayley–Menger matrix $M(p_1, \dots, p_n)$ (defined analogously to the right side of Eq. (12) but without the determinant operation) is at most $m + 1$.*

A direct application of the theorem leads to that, in 2D

$$D(p_1, p_2, p_3, p_4) = 0. \quad (13)$$

Combining Eqs. (13) and (11), a nonlinear equation for α can be obtained:

$$h(\alpha) = \begin{vmatrix} 0 & C_{12}^{-2/\alpha} & C_{13}^{-2/\alpha} & C_{14}^{-2/\alpha} & 1 \\ C_{12}^{-2/\alpha} & 0 & C_{23}^{-2/\alpha} & C_{24}^{-2/\alpha} & 1 \\ C_{13}^{-2/\alpha} & C_{23}^{-2/\alpha} & 0 & C_{34}^{-2/\alpha} & 1 \\ C_{14}^{-2/\alpha} & C_{24}^{-2/\alpha} & C_{34}^{-2/\alpha} & 0 & 1 \\ 1 & 1 & 1 & 1 & 0 \end{vmatrix} = 0, \quad (14)$$

where $C_{ij} = P_{ij}/P_0, 1 \leq i < j \leq 4$, and the C_{ij} are all known. An analytical solution to Eq. (14) is difficult to find. However, Eq. (14) can be conveniently solved using the bracketing and bisection numerical technique [25, Section 9.1]. The correctness of the numerical technique has been validated by removing the noise term from Eq. (1), the numerical technique can give the exact value of α . A gradual increase in the standard deviation of the noise term results in a larger and larger estimation error.

Unfortunately, the estimate of α obtained using this method shows a strong bias, i.e., the bias

$$B_{\hat{\alpha}} = E(\hat{\alpha}) - \alpha \quad (15)$$

is certainly nonzero and not a small fraction of α . Fig. 3 shows a histogram of the estimated path loss exponent. The same parameters used in the last section have been used here. The figure is obtained from 10,000 different quadrilaterals whose vertices are uniformly distributed in a square region of 15×15 . It should be noted that in the presence of noise in power measurements, Eq. (14) may have nonunique solutions even in the typical range of α for some quadrilaterals. In that case, we simply discard that quadrilateral and do not use it in the calculation to avoid any ambiguity. In the various simulations shown in this paper, the number of quadrilaterals discarded accounts for about 15% of the total number of quadrilaterals. For the example shown in the figure, the true value of α is 2.3 and the estimated value of α has a bias of 2.08. The

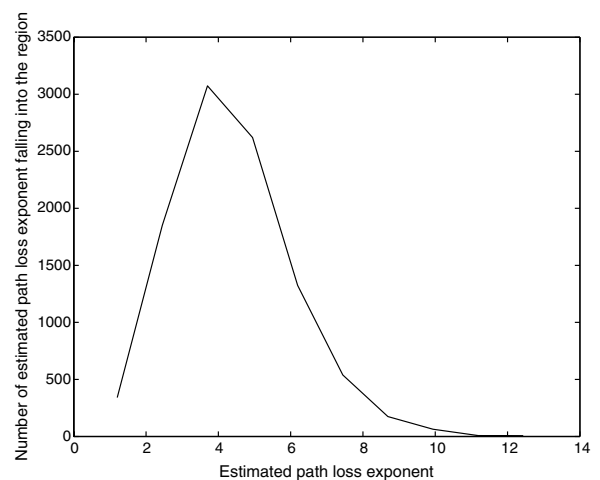


Fig. 3. Histogram of the estimated path loss exponent using Cayley–Menger determinant. The figure is obtained using 10,000 quadrilaterals whose vertices are uniformly distributed in a square region of 15×15 .

simulation shows that $\hat{\alpha}$ obtained using Eq. (14) has a strong bias which cannot be ignored.

Bias removal requires an analysis on $E(\hat{\alpha})$. However, a direct analysis of $E(\hat{\alpha})$ is difficult because of the difficulty in obtaining an explicit analytical expression of α from Eq. (14). Therefore, we resort to numerical experiments to evaluate $E(\hat{\alpha})$. Fig. 4 shows the relationship between the bias of $\hat{\alpha}$ (i.e.,

$B_{\hat{\alpha}}$), the standard deviation of noise in power measurement σ_{dB} , and α . Fig. 5 shows the corresponding relationship between $E(\hat{\alpha})$, σ_{dB} , and α . Both figures are obtained using 3000 quadrilaterals whose vertices are uniformly distributed in a square of 15×15 . The power measurements are obtained using Eqs. (1) and (2). Fig. 6 shows the relationship between $\sigma_{\hat{\alpha}}$, σ_{dB} , and α . The parameter $\sigma_{\hat{\alpha}}$ is the

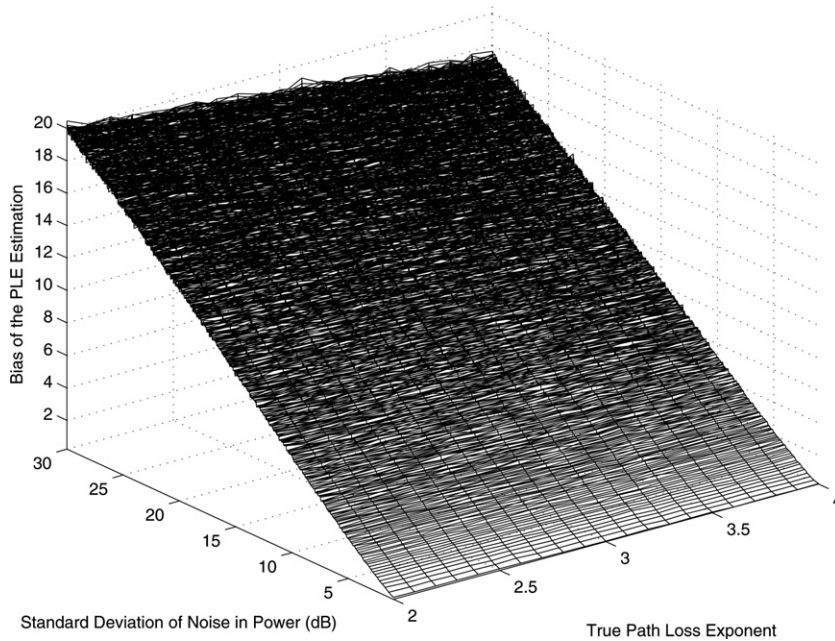


Fig. 4. Relationship between the bias of $\hat{\alpha}$, the standard deviation of noise in power measurement σ_{dB} and α . $B_{\hat{\alpha}}$ depends on α as well as on σ_{dB} .

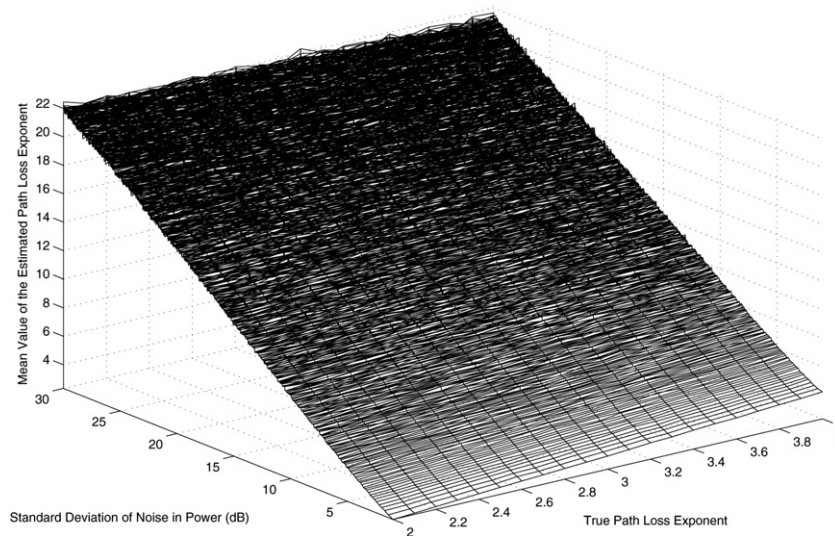


Fig. 5. Relationship between $E(\hat{\alpha})$, the standard deviation of noise in power measurement σ_{dB} and α . $E(\hat{\alpha})$ depends on α as well as on σ_{dB} .

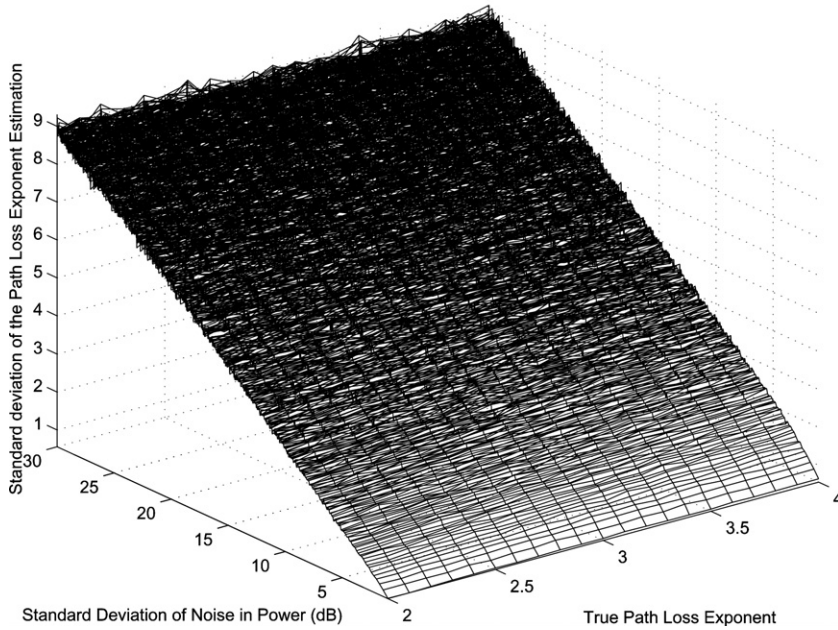


Fig. 6. Relationship between the standard deviation of $\hat{\alpha}$, the standard deviation of noise in power measurement σ_{dB} and α . $\sigma_{\hat{\alpha}}$ depends on σ_{dB} , and to a small degree on α as well. At larger values of σ_{dB} , $\sigma_{\hat{\alpha}}$ is almost independent of α . The dependence of $\sigma_{\hat{\alpha}}$ on α is more significant with smaller values of σ_{dB} .

square root of the sample variance of $\hat{\alpha}$. With a little bit abuse of terminology, we call $\sigma_{\hat{\alpha}}$ the standard deviation of $\hat{\alpha}$.

Fig. 7 shows the relationship between $E(\hat{\alpha})$ and σ_{dB} at specific values of $\alpha = 2.0$, $\alpha = 3.0$ and $\alpha = 4.0$. Fig. 8 shows the relationship between $\sigma_{\hat{\alpha}}$ and σ_{dB} at specific values of $\alpha = 2.0$, $\alpha = 3.0$ and $\alpha = 4.0$.

Further simulations show that the relationships between $E(\hat{\alpha})$, σ_{dB} and α , and between $\sigma_{\hat{\alpha}}$, σ_{dB} and

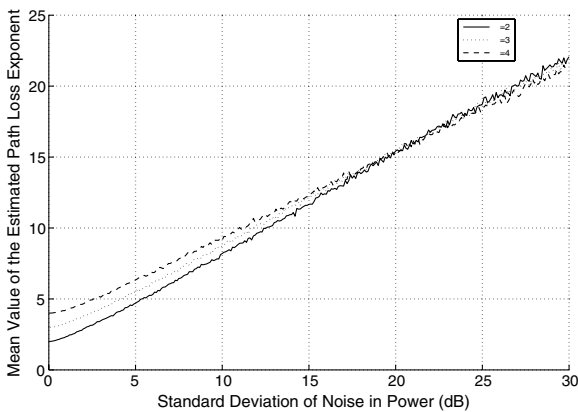


Fig. 7. Relationship between $E(\hat{\alpha})$ and the standard deviation of noise in power measurement σ_{dB} at specific values of $\alpha = 2.0$, $\alpha = 3.0$ and $\alpha = 4.0$.

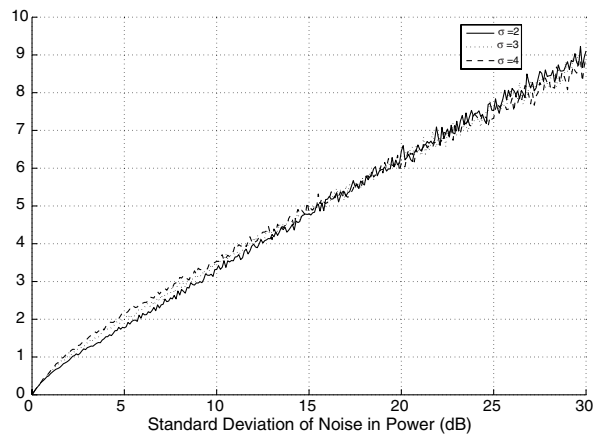


Fig. 8. Relationship between the standard deviation of $\hat{\alpha}$ and the standard deviation of noise in power measurement σ_{dB} at specific values of $\alpha = 2.0$, $\alpha = 3.0$ and $\alpha = 4.0$.

α , are almost independent of the distribution of the vertices of the quadrilaterals, and independent of the shape of the area in which the vertices of the quadrilaterals are located. These are shown in Figs. 9 and 10. Fig. 9 shows the relationship between $E(\hat{\alpha})$, σ_{dB} and α for quadrilaterals whose vertices are located in areas of a variety of different shapes and distributed in the area following different distributions. This relationship between $E(\hat{\alpha})$, σ_{dB} and α is

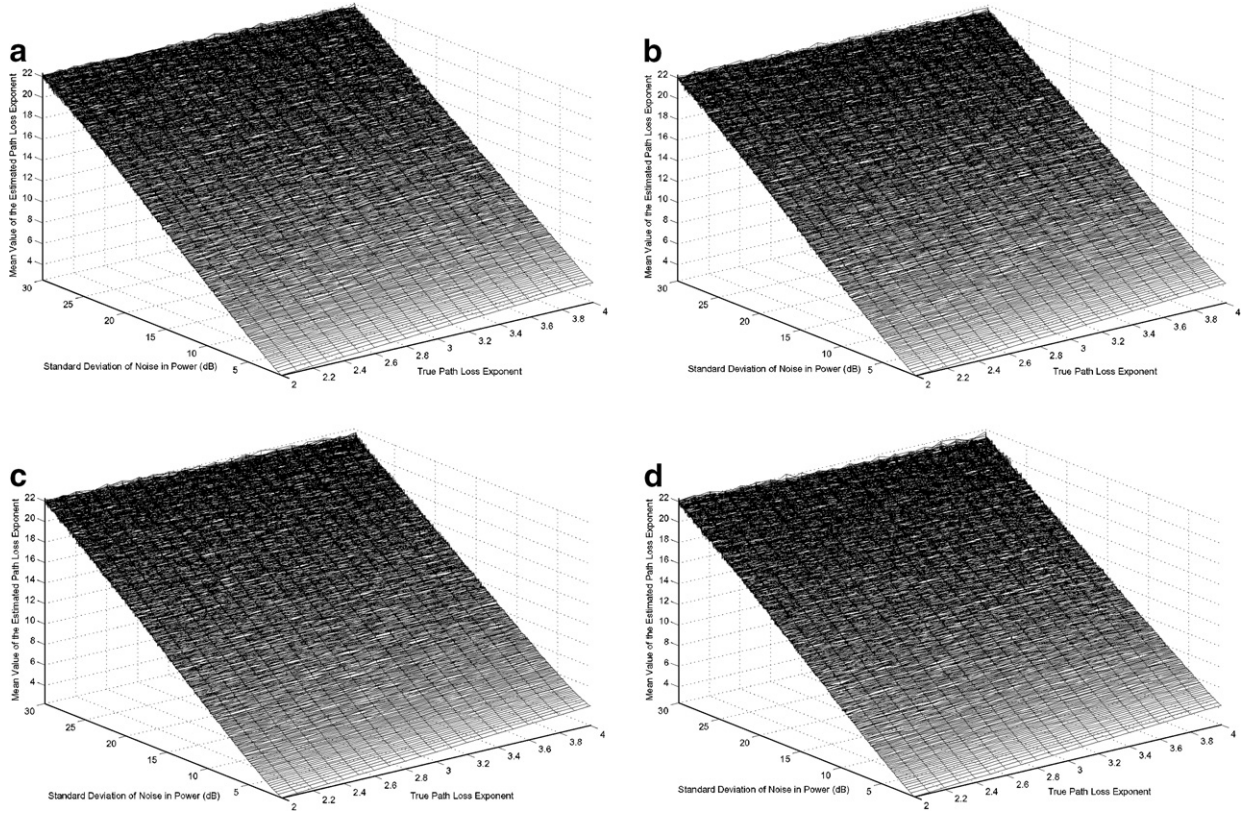


Fig. 9. Relationship between the bias of $E(\hat{\alpha})$, σ_{dB} and α . The relationship between $E(\hat{\alpha})$, σ_{dB} and α is almost independent of the distribution of the vertices of the quadrilaterals and independent of the shape of the area in which the vertices of the quadrilaterals are located. (a) Generated from 3000 quadrilaterals whose vertices are uniformly distributed in a “L” shaped area. (b) Generated from 3000 quadrilaterals whose vertices are uniformly distributed in a rectangular area of 10×20 . (c) Generated from 3000 quadrilaterals whose vertices are distributed in a square area of 15×15 following a truncated Gaussian distribution with a zero mean and a standard variation of 5. (d) Generated from 3000 quadrilaterals whose vertices are located in a ring. The inner radius of the ring is 5 and the outer radius is 10. The coordinates of the vertices are generated by first selecting a number uniformly distributed in $[5, 10]$ and then selecting a number uniformly distributed in $[0, 2\pi]$. The two numbers are used as the polar coordinate of the vertex to obtain the rectangular coordinate.

explored in Section 4 to approximately correct the bias in $E(\hat{\alpha})$. Fig. 10 shows the relationship between $\sigma_{\hat{\alpha}}$, σ_{dB} and α . This relationship between $\sigma_{\hat{\alpha}}$, σ_{dB} and α is further explored in Section 5.

4. Path loss exponent estimation based on pattern matching

Based on the observation shown in Fig. 9 that the relationship between $E(\hat{\alpha})$, σ_{dB} and α is independent of the distribution of the vertices of various quadrilaterals and the shape of the area in which vertices of the quadrilaterals are located, a pattern matching technique can be used to estimate the path loss exponent using the power measurements only.

Specifically, via a priori simulation, a data base can be established where each entry in the data base

is arranged in the form $(\alpha_i, \sigma_{dB,j}^2, E(\hat{\alpha})_{\alpha_i, \sigma_{dB,j}^2})$. The symbol $E(\hat{\alpha})_{\alpha_i, \sigma_{dB,j}^2}$ is used to emphasize dependence of $E(\hat{\alpha})$ on the path loss exponent α_i and the variance of noise in power measurements $\sigma_{dB,j}^2$. This data base can be obtained using a large number of quadrilaterals whose vertices, say, are uniformly distributed in an area. The corresponding power measurements are obtained using Eqs. (1) and (2). The distance between adjacent σ_{dB}^2 is the same, i.e.,

$$\sigma_{dB,j+1}^2 - \sigma_{dB,j}^2 = \Delta\sigma_{dB}^2. \tag{16}$$

The distance between adjacent α is also the same, i.e.,

$$\alpha_{i+1} - \alpha_i = \Delta\alpha. \tag{17}$$

The parameters $\Delta\sigma_{dB}^2$ and $\Delta\alpha$ are empirically chosen constants, which do not change with i and j .

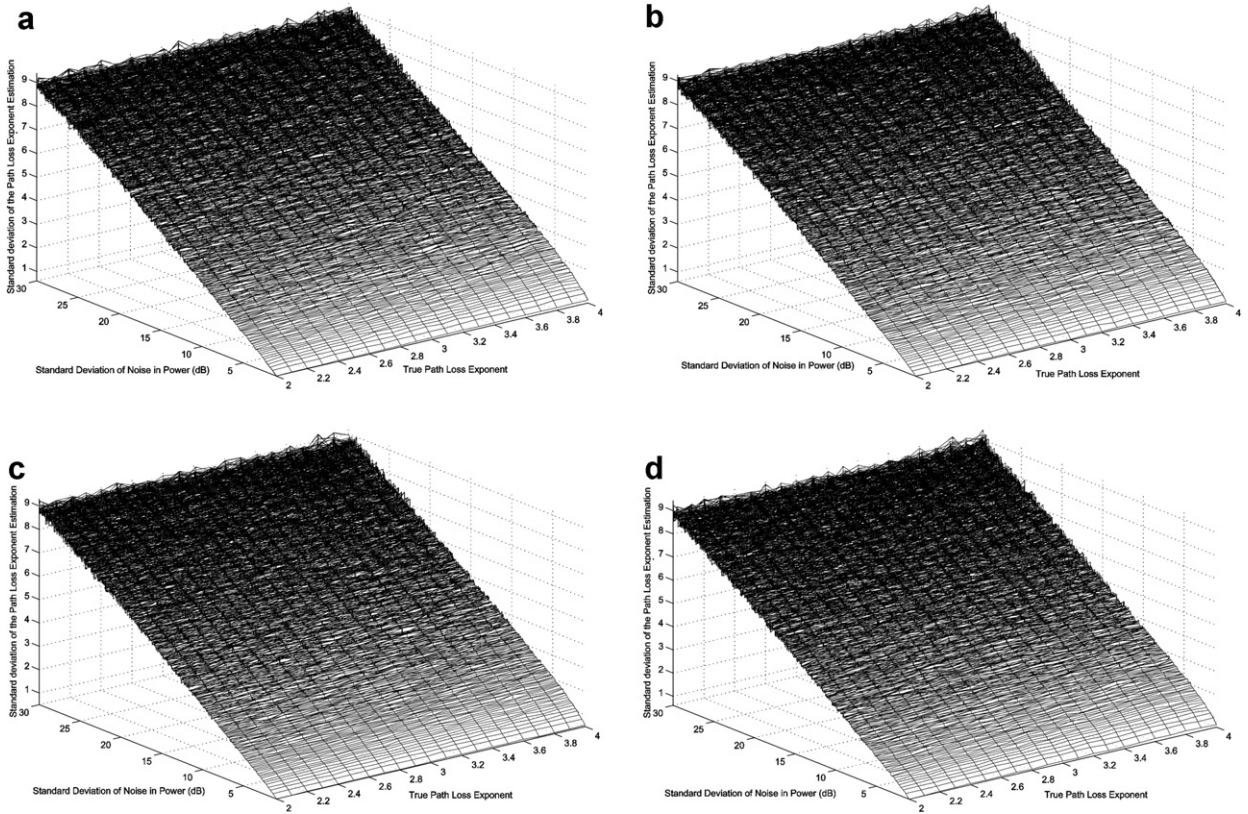


Fig. 10. Relationship between $\sigma_{\hat{\alpha}}$, σ_{dB} and α . The relationship between $\sigma_{\hat{\alpha}}$, σ_{dB} and α is almost independent of the distribution of the vertices of the quadrilaterals and independent of the shape of the area in which the vertices of the quadrilaterals are located. Sub-figures (a)–(d) are obtained under the same conditions as those in Fig. 9.

Given this data base, the estimation of α can be obtained using the following procedure for pattern matching:

1. Identify a set of fully connected quadrilaterals in the wireless sensor network for further computation.
2. Add a random Gaussian noise with variance $\Delta\sigma_{\text{dB}}^2$ into each power measurement. The power is measured in dB milliwatts unit.
3. For each individual quadrilateral, solve for $\hat{\alpha}$ using Eq. (14). An $E(\hat{\alpha})_{r,1}$ corresponding to $\Delta\sigma_{\text{dB}}^2$ can be obtained as the average value of $\hat{\alpha}$ obtained from each individual quadrilateral. Here the subscript r is used to mark the difference with the corresponding value in the database.
4. Repeat steps 2 and 3 using different noise variance values $M\Delta\sigma_{\text{dB}}^2$, where $M = 0, 1, 2, \dots, m$. Here, $M = 0$ corresponds to the original data set without the additionally introduced noise. A series of tuples $(0, E(\hat{\alpha})_{r,0}), (\Delta\sigma_{\text{dB}}^2, E(\hat{\alpha})_{r,1}), \dots, (m\Delta\sigma_{\text{dB}}^2, E(\hat{\alpha})_{r,m})$ can then be obtained.

5. Search the database and find the values of i and j such that:

$$\{i, j\} = \arg \min_{\{i, j\}} \sum_{N=0}^m (E(\hat{\alpha})_{r,N} - E(\hat{\alpha})_{\alpha_i, \sigma_{\text{dB},j+N}^2})^2. \tag{18}$$

The parameter m has to be a large number, say ≥ 500 , in order to obtain a reasonably accurate estimate of α , which is robust against the randomness in the data. As will be shown in the next section, the accuracy of the path loss exponent estimation can be increased by choosing a larger value of m and smaller values of $\Delta\sigma_{\text{dB}}^2$ and $\Delta\alpha$.

6. Finally, an improved estimate of α approximately correcting for the bias can be obtained as

$$\hat{\alpha} = \alpha_i. \tag{19}$$

Similarly, an estimate of σ_{dB} can be obtained as

$$\hat{\sigma}_{\text{dB}} = \sigma_{\text{dB},j}. \tag{20}$$

4.1. Simulation validation

In this section, we shall validate the proposed technique using both simulations and real measurements. The database is established by simulations using 3000 quadrilaterals whose vertices are uniformly distributed in a square region of 15×15 . The measured power is generated using Eqs. (1) and (2). $\Delta\sigma_{dB}^2$ is set to be 1 and the distance between adjacent α_i is set to be 0.1, i.e., $\Delta\alpha = 0.1$. Another set of 3000 quadrilaterals whose vertices are uniformly distributed in a rectangular area of 10×20 are used to establish the performance of the proposed algorithm. 700 points are used in the search, i.e., $m = 700$ in Eq. (18). The simulation is repeated by varying the value of α from 2 to 4 and varying the value of σ_{dB} from 5 to 10, which are the typical ranges of the two parameters [11]. Fig. 11 shows the empirical cumulative distribution function (CDF) of error in estimating α and Fig. 12 shows the the empirical CDF of error in estimating σ .

As shown in Fig. 11, the error in estimating α is contained in the region $[-0.3, 0.1]$. The mean estimation error is -0.1175 and the error variance is 0.0115. Fig. 12 shows that the error in estimating σ_{dB} is contained in the region $[0, 1]$. The mean estimation error is 0.4827 and the error variance is 0.0263. The estimation error is attributable to the randomness in the data but can be reduced by using smaller values of $\Delta\sigma_{dB}^2$ and $\Delta\alpha$ at the expense of increased computational load. For example, our simulation shows that by using $m = 2800$, $\Delta\alpha = 0.05$ and $\Delta\sigma_{dB}^2 = 0.25$, the maximum error in

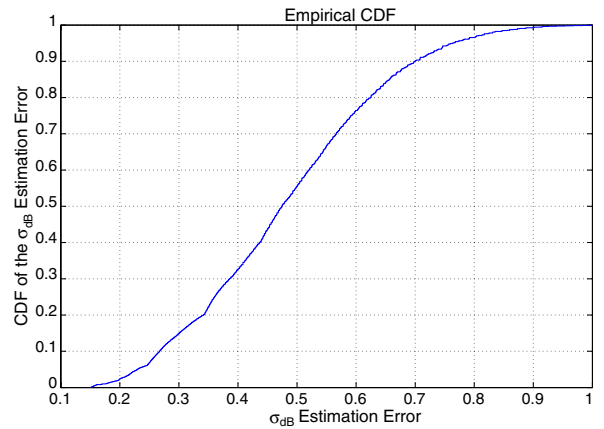


Fig. 12. The empirical CDF of error in estimating σ_{dB} using the pattern matching technique. The vertices of the quadrilaterals are uniformly distributed in a rectangular area of 10×20 .

estimating α reduces to 0.2. The mean error reduces to -0.0603 and the error variance reduces to 0.0056.

Simulations using quadrilaterals whose vertices are distributed in an area of a different shape and/or following a different distribution show similar performance. Figs. 13 and 14 show the simulation results using a set of 3000 quadrilaterals whose vertices are distributed in a square region of 15×15 following a truncated two-dimensional Gaussian distribution. The mean of the Gaussian distribution is at the center of the square region and the standard deviation of the Gaussian distribution is 5. Both figures show similar performance as those in Figs. 11 and 12 except that the estimation error of α has a value of -0.4 at a couple of points in Fig. 13. The

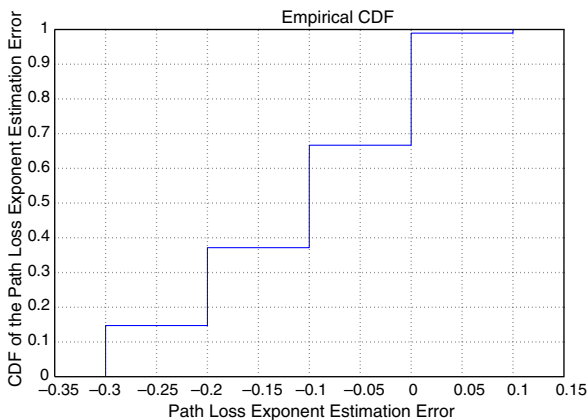


Fig. 11. The empirical CDF of error in estimating α using the pattern matching technique. The vertices of the quadrilaterals are uniformly distributed in a rectangular area of 10×20 .

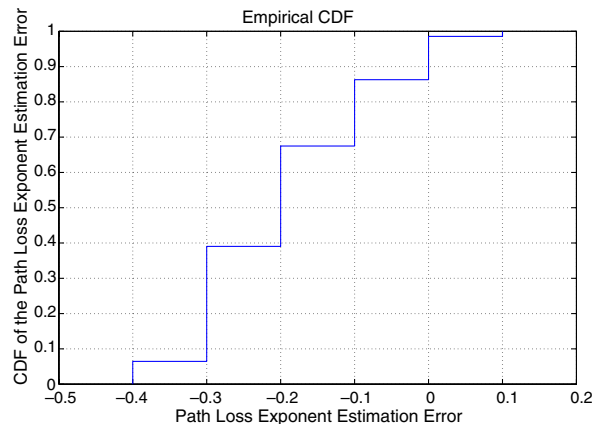


Fig. 13. The empirical CDF of error in estimating α using the pattern matching technique. The vertices of the quadrilaterals are distributed in a square region of 15×15 following a truncated two-dimensional Gaussian distribution.

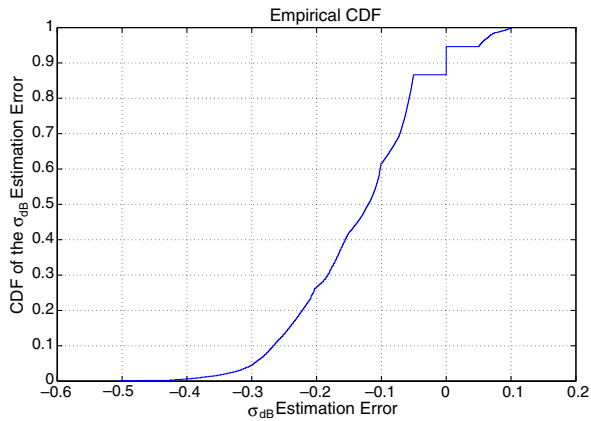


Fig. 14. The empirical CDF of error in estimating σ_{dB} using the pattern matching technique. The vertices of the quadrilaterals are distributed in a square region of 15×15 following a truncated two-dimensional Gaussian distribution.

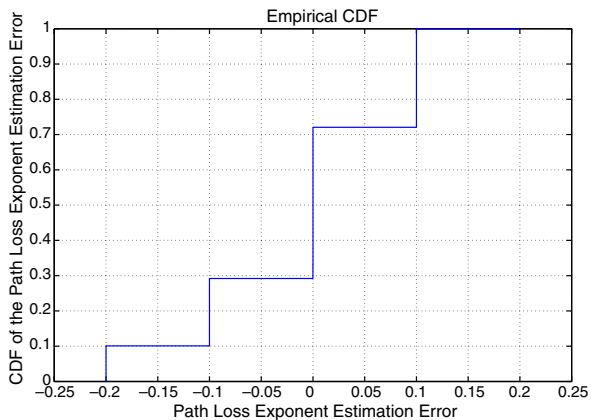


Fig. 15. The empirical CDF of error in estimating α using the pattern matching technique. The vertices of the quadrilaterals are drawn randomly from nodes distributed in a rectangular region of 10×15 following a Poisson distribution with a uniform node density of $100/(10 \times 15)$.

mean error in estimating α is -0.1785 . The estimation error of σ_{dB} is better than that in Fig. 12 and the mean estimation error is -0.1252 . Figs. 15 and 16 show the simulation results using a set of 3000 quadrilaterals whose vertices are distributed in a rectangular region of 10×15 following a Poisson distribution. The mean error in estimating α is -0.0113 and the mean estimation error of σ_{dB} is 0.1021 .

4.2. A comparison with a MLE of the PLE using both power and distance measurements

To further evaluate the performance of the proposed technique, we apply the proposed PLE esti-

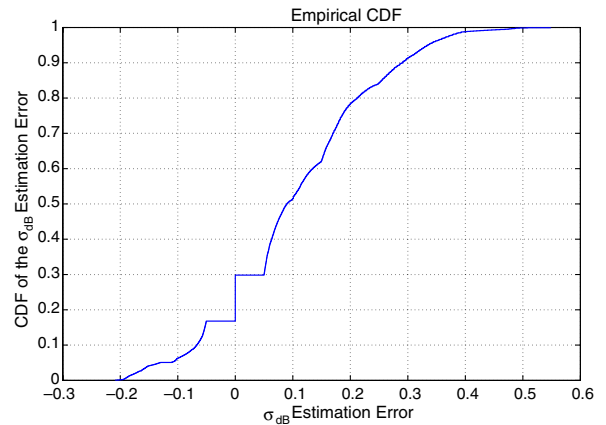


Fig. 16. The empirical CDF of error in estimating σ_{dB} using the pattern matching technique. The vertices of the quadrilaterals are drawn randomly from nodes distributed in a rectangular region of 10×15 following a Poisson distribution with a uniform node density of $100/(10 \times 15)$.

mation technique to real measurement data and compare the PLE estimate obtained using the proposed technique with that in [1] which obtains a maximum likelihood estimate of the PLE using both power measurements and distance measurements. The measurement data and the deployment of sensors can also be found at <http://www.eecs.umi-ch.edu/~hero/localize/>. The wireless sensor network in [1] consists of 44 fully connected nodes, which make up 135,751 quadrilaterals. It is both computationally intensive and unnecessary to compute $\hat{\alpha}$ for each quadrilateral. Here, we randomly choose 10,000 quadrilaterals for computation. The reference power $P_0(d_0)$ [dBm] is calculated using the free space Friis equation at a reference distance $d_0 = 1m$ and $P_0(d_0)$ [dBm] = -37.4663 dBm [1]. The PLE estimated using the proposed technique is 2.2. Using both power measurements and distance measurements (946 distance measurements and 946 power measurements from 44 fully connected nodes), a maximum likelihood estimate of the PLE is shown to be 2.3022 [1]. Assuming the PLE estimate obtained using both power measurements and distance measurements represents the true value of PLE, the PLE estimate obtained using the proposed technique which does not use distance measurements has an estimation error of -0.1022 . The true value of σ_{dB} (i.e., the value obtained using both power measurements and measured distances) is 3.92 and the estimation error is -1.50 . The slightly larger error in estimating σ_{dB} when using real measurement data may be attributable to a deviation of

the density of the noise in the power measurements from a Gaussian distribution.

As a further comparison of the proposed technique with the maximum likelihood estimator using both power and distance measurements, we analyze the number of distance measurements required by the maximum likelihood estimator to make a PLE estimate with a similar accuracy as the proposed technique. Given k distance measurements d_1, d_2, \dots, d_k (recall that all distances are normalized with regards to known distance d_0) and the corresponding power measurements P_1 [dBm], P_2 [dBm], \dots , P_k [dBm], it can be readily shown from Eqs. (1) and (2) that a maximum likelihood estimate of the PLE is:

$$\hat{\alpha}_m = \frac{-\sum_{i=1}^k (P_i \text{ [dBm]} - P_0 \text{ [dBm]}) \log_{10} d_i}{10 \sum_{i=1}^k (\log_{10} d_i)^2}. \quad (21)$$

According to Eqs. (1) and (2), P_i [dBm] is related to d_i by:

$$P_i \text{ [dBm]} = P_0 \text{ [dBm]} - 10\alpha \log_{10} d_i + n_i, \quad (22)$$

where the sequence $\{n_i\}$ is a stationary zero mean white Gaussian sequence of random variables with standard deviation σ_{dB} . Replacing P_i [dBm] in Eq. (21) with Eq. (22), it can be shown that

$$\hat{\alpha}_m = \alpha - \frac{\sum_{i=1}^k n_i \log_{10} d_i}{10 \sum_{i=1}^k (\log_{10} d_i)^2}, \quad (23)$$

and

$$E(\hat{\alpha}_m - \alpha)^2 = \frac{\sigma_{dB}^2}{100 \sum_{i=1}^k (\log_{10} d_i)^2}. \quad (24)$$

Eq. (24) shows that the mean square error of the estimated PLE depends on the distribution of distances. Considering a simple scenario of k distance measurements uniformly distributed between 1 and 10, i.e., $d_i = 1 + 9i/k$, Eq. (24) becomes

$$E(\hat{\alpha}_m - \alpha)^2 = \frac{\sigma_{dB}^2}{100 \sum_{i=1}^k (\log_{10}(1 + 9i/k))^2}. \quad (25)$$

Fig. 17 shows the variation of the mean square error of the estimated PLE with σ_{dB} and number of distance measurements. Using the performance of the proposed technique shown in Fig. 11 for example, the mean square error of the estimated PLE, i.e., the sum of the square of the mean estimation error and the error variance, is 0.025. When σ_{dB} is equal to 5, the maximum likelihood estimator using both power and distance measurements needs 18 distance measurements to achieve a similar accuracy as the proposed technique. A larger number of distance

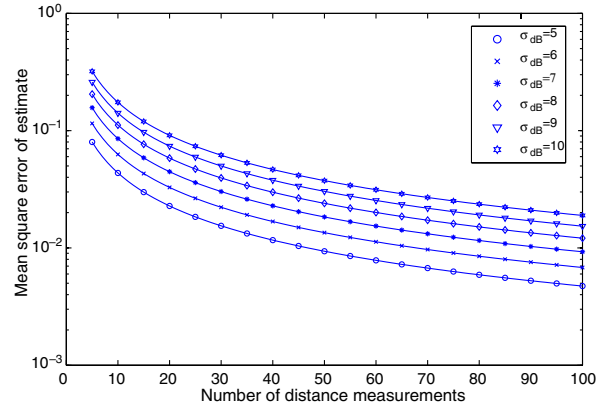


Fig. 17. Variation of the mean square error of the estimated PLE with σ_{dB} and number of distance measurements. The PLE is obtained from a maximum likelihood estimator using both power and distance measurements.

measurements is required at a larger value of σ_{dB} and the converse.

In addition to not requiring distance measurements, another advantage of the proposed technique is it makes the PLE estimation possible in hostile, dangerous or inaccessible environments. Note that even in the same environment, the channel characteristics may change considerably over a long period of time due to seasonal changes and weather changes [11], the proposed technique also show advantage for implementation in these environments.

4.3. A discussion on the computational complexity and the impact of the PLE estimation error

In this section, we have a brief discussion of the computational complexity of the proposed technique and the impact of the PLE estimation error on sensor network localization.

To evaluate the computational complexity of the proposed algorithm, further simulations are performed to estimate the number of quadrilaterals required in order to obtain a stable performance. The simulation results are shown in Fig. 18. Fig. 18 shows that a minimum of 1000 quadrilaterals are required in order for the proposed algorithm to achieve a stable performance.

In the proposed algorithm, the data base required for pattern matching can be established via a priori simulation. The memory space required for storing the data base is in the order of hundreds of kilo-bytes which is not a major constraint for the implementation of the proposed algorithm.

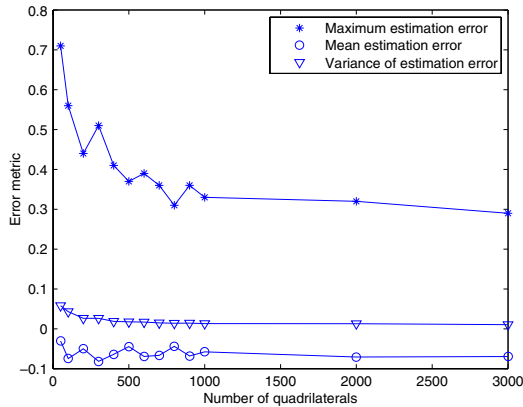


Fig. 18. Variation of the maximum estimation error of $\hat{\alpha}$, mean estimation error and error variance with number of quadrilaterals used in the simulation. Each point shown in the figure is the average value of ten simulations using different random seed. The vertices of the quadrilaterals are drawn randomly from nodes distributed in a rectangular region of 10×15 following a Poisson distribution with a uniform node density of $100/(10 \times 15)$.

However the online computation involving 1000 quadrilaterals and the pattern matching may present a major challenge for distributed implementation of the proposed algorithm. Therefore the proposed algorithm in its present form is not suitable for implementation in a distributed environment. In a centralized environment, the proposed algorithm can be implemented in a central station or in a cluster head which has more energy and computation power than an ordinary sensor node. It remains a future research topic to design a distributed algorithm in which each sensor does the computation for the quadrilateral it resides in and an improved estimate of PLE is obtained by fusing the computation results of individual sensors.

The impact of the PLE estimation error on the estimation of individual inter-sensor distances can be readily evaluated. The answer to the more involved question of the impact of the PLE estimation error on sensor network localization is actually linked to a fundamental question: what is the impact of error in distance measurements on the performance of distance-based localization algorithm? Numerous localization algorithms have shown via simulations that the impact of distance measurement error possibly depends on a number of factors which include the distribution of anchors (i.e., sensor nodes with known positions) and non-anchor (i.e., sensor nodes whose positions are to be estimated) nodes, node degree (or equivalently node density and sensing range) and the shape of the area in which sensors are deployed [14]. We

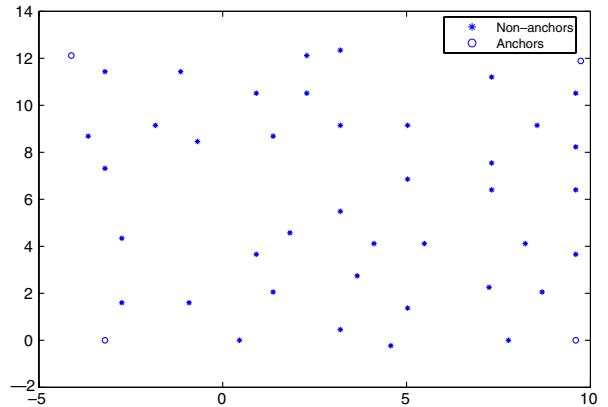


Fig. 19. True positions of anchors and non-anchor nodes in the simulation.

are yet to develop an accurate knowledge in the area. In this paper, instead of giving a comprehensive evaluation of the impact of PLE estimation error on sensor network localization, we give an illustration of the possible impact of the PLE estimation error using the measurement data in [1]. The wireless sensor network in [1] consists of 44 fully connected nodes. The four sensors located at the four corners are chosen to be the anchor nodes and the rest are the non-anchor nodes. Fig. 19 shows the placement of these sensors. The true value of PLE is 2.3022 [1]. An error term varying from -0.4 to 0.4 is added to the true value to evaluate the impact of the PLE estimation error. The sum of the true PLE and the error is termed as the estimated PLE, i.e., $\hat{\alpha}$. The sensor network localization is formulated as the following optimization problem:

$$\begin{aligned} \{\hat{x}_{i,m < i \leq n}\} = \arg \min_{\{\hat{x}_{i,m < i \leq n}\}} & \\ \times \sum_{i=m+1}^n \sum_{j \in N_i} (P_{ij} - 10\hat{\alpha} \log_{10} \|\hat{x}_i - \hat{x}_j\|)^2, & \end{aligned} \quad (26)$$

where anchor nodes are numbered from 1 to m , non-anchor nodes are numbered from $m+1$ to n , N_i denotes the set of neighbors of node i and $\|\cdot\|$ denotes the Euclidean norm. \hat{x}_i and x_i are the estimated position and the true position of the i th sensor respectively and for anchor nodes $\hat{x}_i = x_i$. The simulated annealing algorithm [26] is used to solve the problem and obtain the estimated positions of non-anchor nodes. Fig. 20 shows the variation of the sensor network position estimation error with the PLE estimation error. As shown in

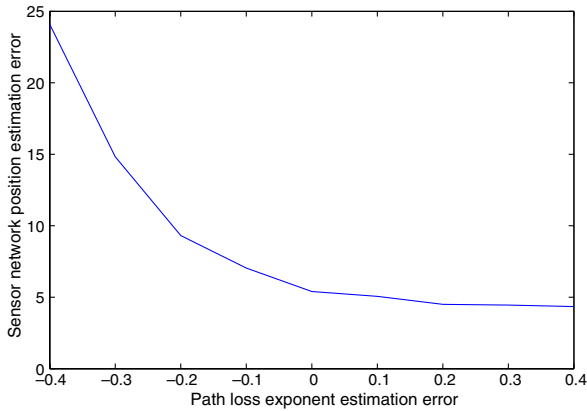


Fig. 20. Variation of the sensor network position estimation error with the PLE estimation error. The sensor network position estimation error shown in the figure is $\frac{1}{n-m} \sum_{i=m+1}^n \|\hat{x}_i - x_i\|^2$, where \hat{x}_i and x_i are the estimated position and the true position of the i th sensor, respectively, sensors 1 to m are anchors, and sensors $m + 1$ to n are non-anchors. Each point shown in the figure is the average value of 10 simulations using different random seed.

the figure, the sensor network localization appears to be more robust against an overestimation of the PLE than an underestimation. Actually, with an overestimation of the PLE, we find a slight improvement in the sensor network localization performance. A plausible explanation of the simulation result is:

- First, the MLE of inter-sensor distance in Eq. (11) is a biased estimate [14] and it tends to overestimate the distance even when the PLE is accurate. A slightly overestimate of the PLE may help to balance this effect.
- Second, this may also be attributable to the placement of anchors and the high node degree of anchors. Given a set of power measurements, an overestimate of the PLE will result in smaller inter-sensor distance estimates. Therefore a “shrinkage” of the estimated sensor positions may occur. However because the anchors are placed at the four corners of the map and they have a high node degree, they constrain the shrinking effect caused by an overestimation of the PLE. This constraint formed by placing the anchors at the corners becomes less effective with an underestimation of the PLE.

5. Further improvement on the proposed technique using data fusion

In Section 4, we presented a technique which approximately corrects the bias of $\hat{\alpha}$ using the rela-

tionship between $E(\hat{\alpha})$, σ_{α} and α . Unsurprisingly a similar technique can also be developed, which begins by establishing a database similar to that in Section 4 but describing the relations between $\sigma_{\hat{\alpha}}$ (instead of $E(\hat{\alpha})$), σ_{α} and α , and uses the pattern matching technique to correct the bias of $\hat{\alpha}$ based on the relationship between $\sigma_{\hat{\alpha}}$, σ_{α} and α . Fig. 21 shows the error in estimating α . The mean estimation error is -0.2597 and the error variance is 0.1295. The same parameters as used in Section 4 are used here.

As shown in the figure, the error in estimating α is significantly worse than that shown in Section 4. This result is expected because in comparison with $E(\hat{\alpha})$, the value of $\sigma_{\hat{\alpha}}$ is less dependent on the value of α , as suggested in Figs. 7 and 8. However the relationship between $\sigma_{\hat{\alpha}}$, σ_{α} and α does provide extra information concerning α , which can be exploited to improve $\hat{\alpha}$ obtained in Section 4 by using data fusion [27].

A popular approach in data fusion is to linearly combine the estimated parameters. Denote the estimated α using the relationship between $\sigma_{\hat{\alpha}}$, σ_{α} and α by $\hat{\alpha}_s$. Denote the estimated α using the relationship between $E(\hat{\alpha})$, σ_{α} and α by $\hat{\alpha}_b$. The dual estimated vector is defined as

$$\vec{\alpha} = [\hat{\alpha}_s, \hat{\alpha}_b]^T. \tag{27}$$

The estimated fusion calculation is given by

$$\hat{\alpha} = \mathbf{W}^T \vec{\alpha}, \tag{28}$$

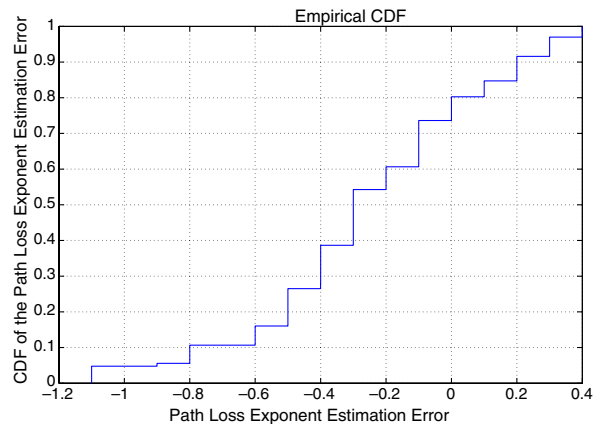


Fig. 21. The empirical CDF of error in estimating α using the pattern matching technique and the relationship between $\sigma_{\hat{\alpha}}$, σ_{α} and α . The vertices of the quadrilaterals are uniformly distributed in a rectangular area of 10×20 .

where \mathbf{W} is a vector in our specific application. In the more general case of simultaneous estimation of multiple parameters, \mathbf{W} is a full rank weight matrix. A typical data fusion approach is to calculate \mathbf{W} such that the sum of the diagonal elements for the error covariance matrix of the fused estimate is minimized. The optimal \mathbf{W} , which gives the lowest error covariance is given by [27]:

$$\mathbf{W} = \mathbf{C}^{-1} \mathbf{A}^T (\mathbf{A} \mathbf{C}^{-1} \mathbf{A}^T)^{-1}. \tag{29}$$

where

$$\mathbf{C} = E \left\{ \begin{bmatrix} \hat{\alpha}_s - \alpha \\ \hat{\alpha}_b - \alpha \end{bmatrix} \begin{bmatrix} \hat{\alpha}_s - \alpha \\ \hat{\alpha}_b - \alpha \end{bmatrix}^T \right\}, \tag{30}$$

and

$$\mathbf{A} = [1 \ 1] \tag{31}$$

in our specific application. α is the corresponding true value. It should be noted that the optimality of data fusion in Eq. (29) relies on the assumptions that covariance is the dominant factor in estimation error in comparison with the bias, and that the estimation errors have a Gaussian distribution [27]. These requirements make the optimality of this data fusion method difficult to prove. However this method is generally robust in the sense that given an accurate error covariance matrix, it always results in a fused estimator with a lower covariance than the individual estimators [28].

To establish the performance improvement of data fusion approach, we use the path loss exponent estimation from the quadrilaterals, whose vertices are distributed in a square region of 15×15 following a truncated two-dimensional Gaussian distribution (as shown in Fig. 13), to obtain the error covariance matrix \mathbf{C} and the weight vector \mathbf{W} . The obtained weight vector is $\mathbf{W} = [-0.1718, 1.1718]^T$. A negative value of -0.1718 indicates that the error in $\hat{\alpha}_s$ and the error in $\hat{\alpha}_b$ are positively correlated. Using this weight vector, we linearly combine the path loss exponent estimates obtained using the relationship between $\sigma_{\hat{\alpha}}$, σ_{dB} and α , and using the relationship between $E(\hat{\alpha})$, σ_{dB} and α (as shown in Eq. (28)).

Fig. 22 shows the path loss exponent estimation error for quadrilaterals, whose vertices are uniformly distributed in a rectangular area of 10×20 . An overall improvement has been achieved in comparison with the results shown in Fig. 11, although at some points the estimation error becomes larger, which can be possibly explained by the statistical

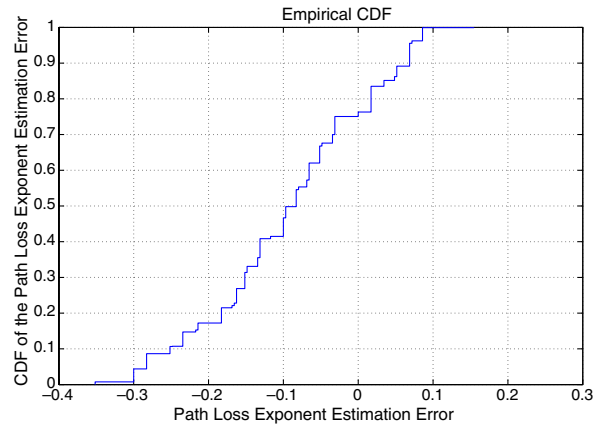


Fig. 22. Error in estimating α using data fusion. The vertices of the quadrilaterals are uniformly distributed in a rectangular area of 10×20 .

nature of data fusion. The mean estimation error reduces from the original -0.1175 to -0.0930 . The error variance remains essentially the same.

6. Conclusions and further work

In this paper, we presented some techniques for online calibration of path loss exponent in wireless sensor networks without relying on distance measurements. Specifically, techniques were proposed which are based on different assumptions about knowledge of distance information.

The first technique assumes that the probability distribution of distance between neighboring sensors is known. Then an algorithm similar to the quantile–quantile plot was proposed, which can estimate the path loss exponent accurately using a small number of received power measurements. However, this assumption of knowing the distance distribution can be unrealistic in some applications. This has motivated us to find a more generic technique without using any distance information.

Then we presented a technique based on the Cayley–Menger determinant, which estimates the path loss exponent using only power measurements and the geometric constraints associated with planarity in a wireless sensor network. The technique can give an accurate estimate of α when there is no noise in power measurements, but it has a large bias in the presence of noise. A pattern matching technique approximately correcting the bias is proposed based on the empirical observation that the relationship between $E(\hat{\alpha})$, σ_{dB} and α is independent of the

distribution of the vertices of various quadrilaterals and the shape of the area in which vertices of the quadrilaterals are located. We also presented an improvement of the earlier technique using data fusion. The proposed algorithms may have significant impact on distance-based wireless sensor network localization, where distance is estimated from the received signal strength measurements.

In this paper, we observed the empirical law that the relationship between $E(\hat{\alpha})$, σ_{dB} and α is independent of the distribution of the vertices of the quadrilaterals and is also independent of the shape of the area in which the vertices of the quadrilaterals are located. It is desirable to obtain an analytical expression of the relationship between $E(\hat{\alpha})$, σ_{dB} and α . This is the direction of our future research.

Furthermore, the proposed algorithm relies on the log-normal propagation model in Eqs. (1) and (2) in the sense that the maximum likelihood estimator shown in Eq. (11) may have a different form when the received signal strength has a different model. Although the log-normal propagation model is a popular model for wireless networks, there are environments in which the log-normal propagation model is not the best model [11,12]. In that case, a technique needs to be developed to select the best model and choose the best estimator for distance to replace Eq. (11) accordingly. Therefore how to develop an algorithm for environments in which the log-normal propagation model does not apply is also a future research topic.

Acknowledgements

This research is supported by National ICT Australia. National ICT Australia is funded by the Australian Government's Department of Communications, Information Technology and the Arts and the Australian Research Council through the *Backing Australia's Ability initiative* and the ICT Centre of Excellence Program.

References

- [1] N. Patwari, I. Hero, A.O.M. Perkins, N. Correal, R. O'Dea, Relative location estimation in wireless sensor networks, *IEEE Transactions on Signal Processing* 51 (8) (2003) 2137–2148.
- [2] P. Bahl, V. Padmanabhan, Radar: an in-building rf-based user location and tracking system, *IEEE INFOCOM 2 (2000) 775–784*.
- [3] P. Bergamo, G. Mazzini, Localization in sensor networks with fading and mobility, in: *The 13th IEEE International Symposium on Personal, Indoor and Mobile Radio Communications*, vol. 2, 2002, pp. 750–754.
- [4] E. Elnahrawy, X. Li, R. Martin, The limits of localization using signal strength: a comparative study, in: *First Annual IEEE Communications Society Conference Sensor and Ad Hoc Communications and Networks*, 2004, pp. 406–414.
- [5] D. Madigan, E. Elnahrawy, R. Martin, W.-H. Ju, P. Krishnan, A. Krishnakumar, Bayesian indoor positioning systems, *IEEE INFOCOM 2005 2 (2005) 1217–1227*.
- [6] D. Niculescu, B. Nath, Localized positioning in ad hoc networks, in: *IEEE International Workshop on Sensor Network Protocols and Applications*, 2003, pp. 42–50.
- [7] P. Prasithsangaree, P. Krishnamurthy, P. Chrysanthis, On indoor position location with wireless lans, in: *The 13th IEEE International Symposium on Personal, Indoor and Mobile Radio Communications*, vol. 2, 2002, pp. 720–724.
- [8] S. Ray, W. Lai, I. Paschalidis, Deployment optimization of sensor-net-based stochastic location-detection systems, *IEEE INFOCOM 2005 4 (2005) 2279–2289*.
- [9] P. Krishnan, A. Krishnakumar, W.-H. Ju, C. Mallows, S. Gamt, A system for lease: location estimation assisted by stationary emitters for indoor rf wireless networks, *IEEE INFOCOM 2 (2004) 1001–1011*.
- [10] T. Roos, P. Myllymaki, H. Tirri, A statistical modeling approach to location estimation, *IEEE Transactions on Mobile Computing* 1 (1) (2002) 59–69.
- [11] T.S. Rappaport, *Wireless Communications: Principles and Practice*, second ed., Prentice-Hall PTR, 2001.
- [12] K. Pahlavan, A.H. Levesque, *Wireless Information Networks*, second ed., Wiley, 2005.
- [13] D. Lymberopoulos, Q. Lindsey, A. Savvides, An empirical analysis of radio signal strength variability in IEEE 802.15.4 networks using monopole antennas, *Technical Report ENA-LAB Technical Report 050501*, 2005.
- [14] G. Mao, B. Fidan, B.D.O. Anderson, "Localization," in: *Sensor Network and Configuration: Fundamentals, Techniques, Platforms and Experiments*. Germany: Springer-Verlag, 2006, pp. 281–316.
- [15] G.M. Crippen, T.F. Havel, *Distance Geometry and Molecular Conformation*, John Wiley and Sons Inc., New York, 1988.
- [16] L.M. Blumenthal, *Theory and Applications Distance Geometry*, Oxford University Press, 1993.
- [17] R. Stoleru, J. Stankovic, Probability grid: a location estimation scheme for wireless sensor networks, in: *First Annual IEEE Communications Society Conference on Sensor and Ad Hoc Communications and Networks*, 2004, pp. 430–438.
- [18] S. Dhillon, K. Chakrabarty, S. Iyengar, "Sensor placement for grid coverage under imprecise detections," in: *Proceedings of the Fifth International Conference on Information Fusion*, vol. 2, 2002, pp. 1581–1587.
- [19] K. Chakrabarty, S. Iyengar, H. Qi, E. Cho, Grid coverage for surveillance and target location in distributed sensor networks, *Computers IEEE Transactions* 51 (12) (2002) 1448–1453.
- [20] L.E. Miller, Distribution of link distances in a wireless network, *Journal of Research of the National Institute of Standards and Technology* 106 (2) (2001) 401–412.
- [21] J.P. Mullen, Robust approximations to the distribution of link distances in a wireless network occupying a rectangular region, *Mobile Computing and Communications Review* 7 (2) (2003).

- [22] C.-C. Tseng, H.-T. Chen, K.-C. Chen, On the distance distributions of the wireless ad hoc networks, in: IEEE VTC Spring, Melbourne, 2006.
- [23] R. Bartoszynski, M. Niewiadomska-Bugaj, Probability and Statistical Inference, ser. Wiley Series in Probability and Statistics, Wiley, 1996.
- [24] R.J. Hyndman, Y. Fan, Sample quantiles in statistical packages, *Am. Stat* 50 (1996) 361–365.
- [25] W.H. Press, S.A. Teukolsky, W.T. Vetterling, B.P. Flannery, Numerical Recipes in C – The Art of Scientific Computing, second ed., Cambridge University Press, 2002.
- [26] A.A. Kannan, G. Mao, B. Vucetic, Simulated annealing based localization in wireless sensor network, in: The 30th IEEE Conference on Local Computer Networks, 2005, pp. 513–514.
- [27] Y. Zhu, Multisensor Decision and Estimation Fusion, ser. The International Series on Asian Studies in Computer and Information Science, Springer, 2002.
- [28] M. McGuire, K.N. Plataniotis, A.N. Venetsanopoulos, Data fusion of power and time measurements for mobile terminal location, *IEEE Transactions on Mobile Computing* 4 (2) (2005) 142–153, 1536–1233.



Guoqiang Mao received the Bachelor degree in electrical engineering, Master degree in engineering and Ph.D. in telecommunications engineering in 1995, 1998 and 2002 respectively. After graduation from PhD, he worked in “Intelligent Pixel Incorporation” as a Senior Research Engineer for one year. He joined the School of Electrical and Information Engineering, the University of Sydney in December 2002 where he is

a Senior Lecturer now. His research interests include wireless sensor networks, wireless localization techniques, network QoS, telecommunications traffic measurement, analysis and modeling, and network performance analysis.



Brian D.O. Anderson was born in Sydney, Australia, and received his undergraduate education at the University of Sydney, with majors in pure mathematics and electrical engineering. He subsequently obtained a Ph.D. degree in electrical engineering from Stanford University. Following completion of his education, he worked in industry in Silicon Valley and served as a faculty member in the Department of Electrical

Engineering at Stanford. He was Professor of Electrical Engi-

neering at the University of Newcastle, Australia from 1967 until 1981 and is now a Distinguished Professor at the Australian National University and Chief Scientist of National ICT Australia Ltd. His interests are in control and signal processing. He is a Fellow of the IEEE, Royal Society London, Australian Academy of Science, Australian Academy of Technological Sciences and Engineering, Honorary Fellow of the Institution of Engineers, Australia, and Foreign Associate of the US National Academy of Engineering. He holds doctorates (honoris causa) from the Université Catholique de Louvain, Belgium, Swiss Federal Institute of Technology, Zürich, Universities of Sydney, Melbourne, New South Wales and Newcastle. He served a term as President of the International Federation of Automatic Control from 1990 to 1993 and as President of the Australian Academy of Science between 1998 and 2002. His awards include the IEEE Control Systems Award of 1997, the 2001 IEEE James H Mulligan, Jr Education and Systems Society in 1992 and 2001, the Bode Prize of the IEEE Control System Society in 1992 and the Senior Prize of the IEEE Transactions on Acoustics, Speech and Signal Processing in 1986.



Baris Fidan received the B.S. degrees in electrical engineering and mathematics from Middle East Technical University, Turkey in 1996, the M.S. degree in electrical engineering from Bilkent University, Turkey in 1998, and the Ph.D. degree in Electrical Engineering-Systems at the University of Southern California, Los Angeles, USA in 2003. After working as a postdoctoral research fellow at the University of Southern California for

one year, he joined the Systems Engineering and Complex Systems Program of National ICT Australia and the Research School of Information Sciences and Engineering of the Australian National University, Canberra, Australia in 2005, where he is currently a researcher. His research interests include autonomous formations, sensor networks, adaptive and nonlinear control, switching and hybrid systems, mechatronics, and various control applications including high performance and hypersonic flight control, semiconductor manufacturing process control, and disk-drive servo systems.